Momentum scalar triple product as a measure of chirality in electron ionization dynamics of strongly driven atoms

G. P. Katsoulis, ¹ Z. Dube, ² P. B. Corkum⁰, ² A. Staudte⁰, ² and A. Emmanouilidou¹

¹Department of Physics and Astronomy, University College London, Gower Street, London WC1E 6BT, United Kingdom ²Joint Attosecond Science Lab of the National Research Council and the University of Ottawa, Ottawa, Ontario K1A 0R6, Canada



(Received 16 August 2022; accepted 28 September 2022; published 17 October 2022)

We formulate a measure that quantifies chirality in single electron ionization triggered in atoms, which are achiral systems. We do so in the context of Ar driven by a different type of optical fields that consists of two noncollinear laser beams giving rise to chirality that varies in space across the focus of the beams. Our computations account for realistic experimental conditions. To define this measure of chirality, we first find the sign of the electron final momentum scalar triple product $\mathbf{p}_x \cdot (\mathbf{p}_y \times \mathbf{p}_z)$ and multiply it with the probability for an electron to ionize with certain values of the momentum components. Then, we integrate over all values of p_x , p_y , p_z . We show this to be a robust measure of chirality in electron ionization triggered by chiral electric fields.

DOI: 10.1103/PhysRevA.106.043109

I. INTRODUCTION

Ultrafast phenomena in chiral molecules triggered by intense, infrared laser pulses are at the forefront of laser-matter interactions [1–5]. While ultrafast chiral processes can be studied using high harmonic generation (HHG) [1,6–10], the underlying recollision mechanism entails that a stronger chiral response comes at the expense of a greatly suppressed high harmonic signal [1]. Hence, photoelectron spectroscopy is a promising route to a robust signal from molecules driven by intense chiral fields [2,3,5,11–13]. However, the sensitivity of chiral photoelectron spectroscopy also struggles with the fact that laser wavelengths are several orders of magnitude larger than the dimensions of molecules, i.e., the chiralities of the optical field and the molecule are incommensurate. Recently, Ayuso et al. proposed a type of optical field which is chiral on the atomic scale [6] and thereby holds the potential for unprecedented chiral sensitivity. The chiral field is synthe sized by combining two orthogonally polarized two-color laser fields in a noncollinear geometry as illustrated in Fig. 1. The noncollinear geometry creates an intensity and ellipticity grating, and thereby causes the chirality of the laser field to spatially vary across the focus. Thus, it is a fundamental challenge for experiments to decipher the signatures of chirality in the photoelectron spectra from these laser fields. Here, we provide a roadmap on how to analyze experimental photoelectron spectra produced from chiral light. To do so, we perform semiclassical simulations of strong-field ionization and take into account the focal volume distribution of the degree of light chirality. To understand chiral electron ionization, we model photoionization of ground state atoms. The latter have spherical symmetry and are intrinsically achiral systems. Thus, the chiral response of the escaping electron that is imprinted on the ionization spectra arises solely from the dynamics triggered by the electric field of the laser. To analyze the resulting photoelectron spectra we identify a measure that

quantifies chirality in electron ionization dynamics ensuing from an atom strongly driven by a chiral electric field. We construct this measure using the probability $P(p_x, p_y, p_z)$ for an electron to ionize with certain values of the momentum components p_x , p_y and p_z . Next, we multiply this probability by the sign of the momentum scalar triple product $\mathbf{p}_x \cdot (\mathbf{p}_y \times \mathbf{p}_z)$. Integrating over the whole range of the components of the momentum, we obtain the following measure of chirality

$$\mathcal{X} = \iiint \operatorname{sign}(\mathbf{p}_x \cdot (\mathbf{p}_y \times \mathbf{p}_z)) P(p_x, p_y, p_z) dp_x dp_y dp_z.$$
(1)

As expected, we find that when performing a cyclic permutation of p_x , p_y and p_z in Eq. (1) the measures of chirality obtained are equivalent. In what follows, we show that \mathcal{X} is a robust measure of chiral electron ionization.

II. METHOD

We demonstrate that \mathcal{X} measures handedness of electron ionization in the context of Ar atoms driven by two non-collinear laser beams, see Fig. 1. Beams 1, 2 propagate on the x-y plane with wave vectors \mathbf{k}_1 , \mathbf{k}_2 forming an angle α with the y axis

$$\mathbf{k}_{1} = k \sin(\alpha) \hat{\mathbf{x}} + k \cos(\alpha) \hat{\mathbf{y}},$$

$$\mathbf{k}_{2} = -k \sin(\alpha) \hat{\mathbf{x}} + k \cos(\alpha) \hat{\mathbf{y}},$$
 (2)

where $k=2\pi/\lambda$. The electric field of each beam consists of two orthogonally polarized ω and 2ω laser fields. The ω field is polarized along the x-y plane and the 2ω along the z axis, while the 2ω field has smaller intensity. The resultant electric field is given by [6]

$$\mathbf{E}(\mathbf{r},t) = 2E_0 \exp\left[-\left(\frac{t}{\tau}\right)^2\right] (E_x \hat{\mathbf{x}} + E_y \hat{\mathbf{y}} + E_z \hat{\mathbf{z}}), \quad (3)$$

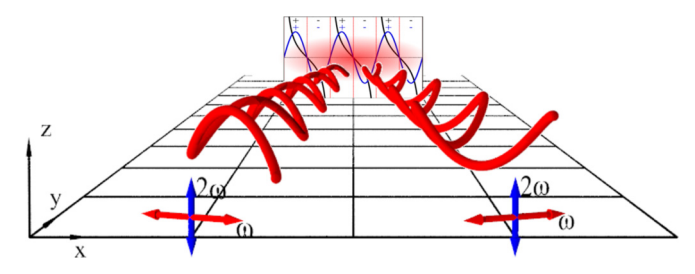


FIG. 1. Schematic plot of two noncollinear laser beams, each consisting of ω -2 ω orthogonally polarized linear fields; ω is polarized on the x-y plane and 2 ω along the z axis. Both beams propagate towards the atom in the focus region (red-shaded ellipse). The resultant electric field has chirality (square inset) that changes along the x axis in the focus region.

where

$$E_{x/y} = \exp\left[-\left(\frac{\rho}{w_0}\right)^2\right] f_{x/y}(x) \cos\left[g(y,t)\right],$$

$$E_z = \exp\left[-\left(\frac{2\rho}{w_0}\right)^2\right] f_z(x) \cos\left[h(y,t)\right],$$
(4)

and

$$f_x(x) = \cos(\alpha)\cos\left[k\sin(\alpha)x + \frac{\phi_2^{\omega} - \phi_1^{\omega}}{2}\right],$$

$$f_y(x) = \sin(\alpha)\sin\left[k\sin(\alpha)x + \frac{\phi_2^{\omega} - \phi_1^{\omega}}{2}\right],$$

$$f_z(x) = r_0\cos\left[2k\sin(\alpha)x + (\phi_2^{2\omega} - \phi_1^{2\omega})\right],$$

$$g(y,t) = k\cos(\alpha)y - \omega t - \frac{\phi_2^{\omega} + \phi_1^{\omega}}{2},$$

$$h(y,t) = 2k\cos(\alpha)y - 2\omega t - (\phi_2^{2\omega} + \phi_1^{2\omega}).$$
 (5)

We note that $\tau=25$ fs and $\tau\sqrt{2\ln(2)}$ is the full width at half maximum of the pulse duration in intensity, while E_0 is the field strength corresponding to intensity 5×10^{13} W/cm². Also, ρ is the radial distance to the propagation axis of each laser beam. Since α is small, 5° , it follows that $\rho\approx\sqrt{x^2+z^2}$. Moreover, $w_0=8.49~\mu m$ is the beam waist of the ω laser field, and r_0^2 is the intensity ratio of 1/100 of the 2ω versus the ω field. Finally, the wavelength λ of the ω field is taken equal to 800 nm. It was previously shown [6] that the resultant electric field is globally chiral if the relative phases of the

 ω and 2ω laser fields in beams 1 and 2, i.e. $\phi_1^{2\omega}-\phi_1^{\omega}$ and $\phi_2^{2\omega}-\phi_2^{\omega}$, satisfy the following condition:

$$(\phi_1^{2\omega} - \phi_1^{\omega}) - (\phi_2^{2\omega} - \phi_2^{\omega}) = \frac{\pi}{2} + n\pi, \text{ with } n \in \mathbb{Z},$$
 (6)

while the resultant electric field is globally achiral when

$$\left(\phi_1^{2\omega} - \phi_1^{\omega}\right) - \left(\phi_2^{2\omega} - \phi_2^{\omega}\right) = n\pi, \quad \text{with } n \in \mathbb{Z}. \tag{7}$$

We compute \mathcal{X} for Ar driven by one of six different resultant electric fields corresponding to six different synthetic pulses. For simplicity, we refer to each resultant electric field of a synthetic pulse as electric field. Each of the six fields, cases 1–6, corresponds to a different combination of $\phi_1^{2\omega} - \phi_1^{\omega}$ and $\phi_2^{2\omega} - \phi_2^{\omega}$ for beams 1 and 2, respectively, see Fig. 2(a). Using Eq. (6) and Eq. (7), we select four globally chiral fields, cases 1, 2, 4, 5, and two globally achiral fields, cases 3, 6, see Fig. 2. In Fig. 2(b), we show that the electric fields which are globally chiral maintain the same handedness along the x axis in the focus region. That is, E_v/E_x and E_z , while keeping y,z,t constant, change sign at the same points in space x. As a result, electric fields 1 and 4 have the same (+) chirality and electric fields 2 and 5 have the same (-) chirality, see Fig. 2(b). Hence, the pairs of electric fields (1, 2) and (4, 5) have opposite chirality. For the globally achiral fields, cases 3 and 6, we find that E_y/E_x and E_z change sign at different points in space x, Fig. 2(b). Hence, the chirality of electric fields 3 and 6 flips sign along the x axis in the focus region, i.e., there is no overall chirality.

A robust measure of chirality \mathcal{X} should have opposite sign for chiral fields of opposite chirality. In this work, the results are presented using the coordinate system defined by the x axis, which is the axis where the electric fields exhibit handedness, and the y axis, which is the propagation axis. In this reference frame, we find that the \mathcal{X} computed from the electron momentum distribution ensuing from each electric field of cases 1-6 has opposite values for opposite chirality fields (1, 2) and (4, 5), while it is zero for achiral fields 3 and 6. We find that another measure of chirality can be obtained when \mathcal{X} is computed using the difference of the normalized electron momenta distributions obtained from two electric fields. Here, we refer to this measure as χd . For instance, considering cases 1–3, we find that Xd computed using chiral field 1 and achiral field 3 has opposite sign from $\mathcal{X}d$ computed using the opposite chirality field 2 and achiral field 3. Hence, the results presented in this work hold true for this natural

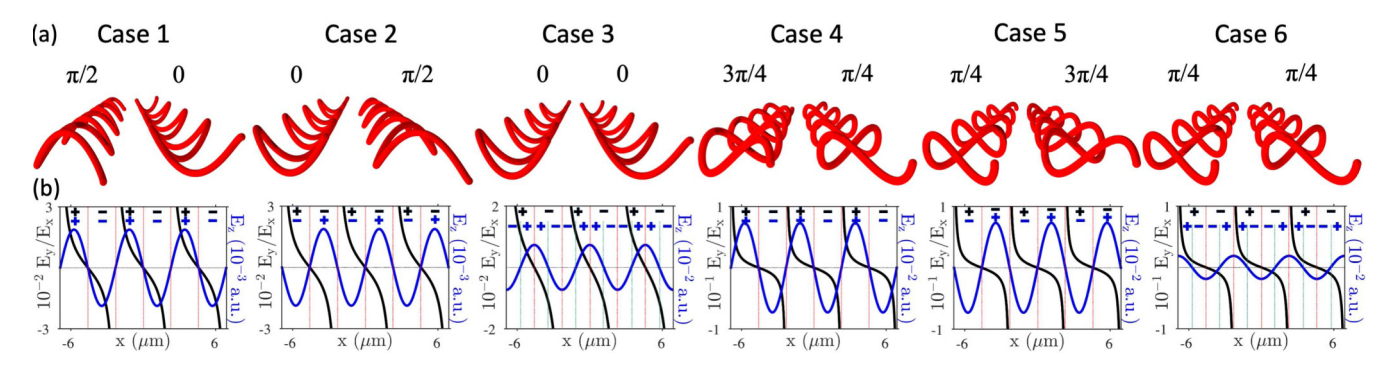


FIG. 2. (a) Schematic plots of six combinations of two noncollinear beams; (b) change of sign of E_y/E_x (black) and E_z (blue) along the x axis in the focus region, at y=z=0, t=T/50. For each case, above beams 1 and 2, we denote $\phi_1^{2\omega}-\phi_1^{\omega}$ and $\phi_2^{2\omega}-\phi_2^{\omega}$ from left to right.

reference frame we employ in this work. Such natural frames have been employed in previous studies of circular dichroism or of magnetic field effects on double ionization due to recollision. In this latter cases, the propagation axis is an axis that plays a pivotal role in identifying asymmetries in ionization observables [14].

We treat single electron ionization of driven Ar by employing a three-dimensional semiclassical model. The only approximation is the initial state. One electron tunnel ionizes through the field-lowered Coulomb-barrier at time t_0 . To compute the tunnel-ionization rate, we employ the quantum mechanical Ammosov-Delone-Krainov formula [15,16]. Using this rate, we select t_0 in the time interval $[-2\tau,2\tau]$. We use parabolic coordinates to obtain the exit point of the tunneling electron along the laser-field direction [17]. We set the electron momentum along the laser field equal to zero, while we obtain the transverse momentum by a Gaussian distribution [15,16]. The microcanonical distribution is employed to describe the initial state of the initially bound electron [18].

Next, we specify at the tunnel-ionization time t_0 the initial conditions for both electrons. Using the three-body Hamiltonian of the two electrons with the nucleus kept fixed, we propagate classically in time the position and momentum of each electron. All Coulomb forces and the interaction of each electron with the electric field in Eq. (3) are fully accounted for with no approximation. To account for the Coulomb singularity, we employ regularized coordinates [19]. Here, we use atomic units.

Previous successes of this model include identifying the mechanism underlying the fingerlike structure in the correlated electron momenta for He driven by 800 nm laser fields [20], see also [21–23]. Moreover, we investigated the direct versus the delayed pathway of nonsequential double ionization for He driven by a 400 nm, long duration laser pulse and achieved excellent agreement with fully *ab initio* quantum mechanical calculations [24]. Also, for low intensities, we have identified a mechanism of double ionization, namely, slingshot non-sequential double ionization [25]. In addition, for several observables of nonsequential double ionization, our results have good agreement with experimental results for Ar when driven by near-single-cycle laser pulses at 800 nm [26].

Next, we describe how we obtain the electron ionization spectra of Ar for each of the six synthetic pulses (cases 1-6). For simplicity, for each case, we set $\phi_2^{\omega} = 0$. Since only the differences $\phi_1^{2\omega} - \phi_1^{\omega}$ and $\phi_2^{2\omega} - \phi_2^{\omega}$ are important, there is no loss of generality. Moreover, for each of the six synthetic pulses, we simulate realistic conditions in a Cold Target Recoil Ion Momentum Spectroscopy (COLTRIMS) or Velocity Map Imaging (VMI) experiment where Ar atoms are at different positions along the x axis in the focus region. To do so, we select 101 equally spaced values of the phase ϕ_1^{ω} in the interval $[0, 2\pi)$. That is, we perform our calculations for each position of the nucleus, i.e., each phase ϕ_1^{ω} . For each ϕ_1^{ω} , we register the single ionization events and obtain the electron ionization spectra. Next, we average over all ϕ_1^{ω} values and obtain the electron spectra $P(p_x, p_y, p_z)$ using at least 10⁷ singly ionizing trajectories. For each synthetic

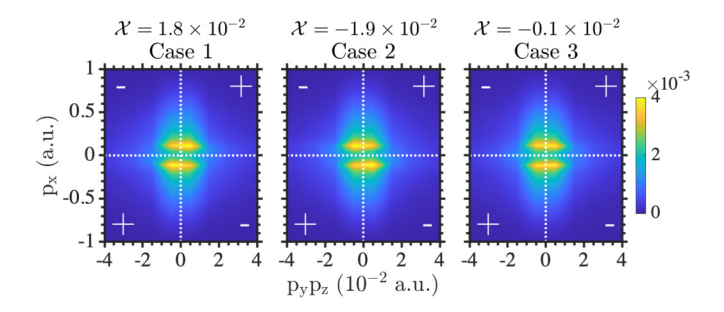


FIG. 3. Probability distribution $P(p_x, p_y, p_z)$ for the electron to ionize with both momentum p_x and the product p_yp_z , for electric fields 1, 2, 3, respectively. The sign in each quadrant corresponds to the sign of $\mathbf{p}_x \cdot (\mathbf{p}_y \times \mathbf{p}_z)$ in this quadrant.

pulse, cases 1–6, the resulting electron spectra are normalized to one.

III. RESULTS

First, we illustrate the measure of chirality \mathcal{X} that is computed separately for each electric field in cases 1–3. To do so, we plot in Fig. 3 the probability distribution $P(p_x, p_y, p_z)$ for an electron to singly ionize with both momentum p_x and the product $p_y p_z$ for the globally chiral fields 1, 2 and the globally achiral field 3. In each quadrant, we assign the sign resulting from the scalar triple product $\mathbf{p}_x \cdot (\mathbf{p}_y \times \mathbf{p}_z)$. We multiply this sign by the distribution $P(p_x, p_y, p_z)$ and sum up over all four quadrants to obtain \mathcal{X} , defined in Eq. (1). We find \mathcal{X} to be equal to 1.8×10^{-2} , -1.9×10^{-2} , -0.1×10^{-2} for electric fields 1, 2, 3, respectively. Indeed, a close inspection of Fig. 3 for case 1 reveals that the probability distribution of the electron momentum p_x and $p_y p_z$ has two lobes with one corresponding to $p_x > 0$ and shifted towards positive values of $p_y p_z$ and another one corresponding to $p_x < 0$ and shifted towards negative values of $p_v p_z$. For case 2, the two lobes are reflected with respect to the $p_y p_z$, consistent with the opposite chirality of fields 1 and 2. Hence, the probability distribution has larger values for case 1 at the first and third quadrants, where $\mathbf{p}_x \cdot (\mathbf{p}_y \times \mathbf{p}_z)$ has a + sign, while for case 2 at the second and fourth quadrants, where $\mathbf{p}_x \cdot (\mathbf{p}_y \times \mathbf{p}_z)$ has a – sign. It follows that \mathcal{X} has a positive (negative) value when Ar is driven by synthetic pulse 1 (2). Also, $|\mathcal{X}|$ is roughly the same for cases 1 and 2. The small offset is due to the statistical error introduced in our computations from the restricted number of single ionization events. This is also supported by ${\mathcal X}$ being equal to -0.1×10^{-2} , instead of zero, when Ar is driven by the achiral field 3.

Next, we illustrate the measure of chirality $\mathcal{X}d$ that is computed using the difference of the normalized electron momenta distributions of two electric fields

$$\mathcal{X}d = \iiint \operatorname{sign}(\mathbf{p}_x \cdot (\mathbf{p}_y \times \mathbf{p}_z)) P^{m,n}(p_x, p_y, p_z) dp_x dp_y dp_z,$$

$$P^{m,n}(p_x, p_y, p_z) = P^m(p_x, p_y, p_z) - P^n(p_x, p_y, p_z),$$
(8)

and P^m/P^n is the probability distribution $P(p_x, p_y, p_z)$ obtained for each of the electric fields 1-6, i.e., m = 1-6 and n = 1-6. In Figs. 4(a1)-4(a3), we plot the probability

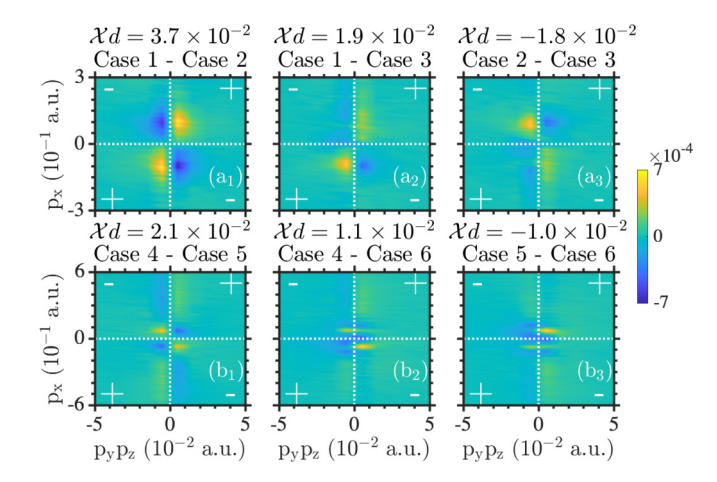


FIG. 4. Probability distribution $P^{m,n}(p_x, p_y, p_z)$. The m,n indexes are 1, 2 for Case 1 and Case 2, 1, 3 for Case 1 and Case 3, 2, 3 for Case 2 and Case 3, 4, 5 for Case 4 and Case 5, 4, 6 for Case 4 and Case 6 and 5,6 for Case 5 and Case 6. The sign in each quadrant corresponds to the sign of $\mathbf{p}_x \cdot (\mathbf{p}_y \times \mathbf{p}_z)$ in this quadrant.

distribution $P^{m,n}(p_x, p_y, p_z)$ for the pair of opposite chirality electric fields (1, 2), i.e., Case 1 - Case 2 [Fig. 4(a1)], and for the pairs of chiral-achiral electric fields (1, 3) and (2, 3), i.e., Case 1 - Case 3 [Fig. 4(a2)] and Case 2 - Case 3 [Fig. 4(a3)]. In each quadrant, we assign the sign resulting from the scalar triple product $\mathbf{p}_x \cdot (\mathbf{p}_y \times \mathbf{p}_z)$. The yellow (blue) color denotes positive (negative) values of $P^{m,n}(p_x, p_y, p_z)$, corresponding to the electron being more (less) probable to ionize with both momentum p_x and the product $p_y p_z$ due to pulse m rather than pulse n. Next, in each quadrant, we multiply the positive or negative values of the distribution (yellow/blue) with the \pm sign of $\mathbf{p}_x \cdot (\mathbf{p}_y \times \mathbf{p}_z)$ and finally sum up. It easily follows that the measure of chirality $\mathcal{X}d$ is larger and positive (3.7×10^{-2}) for the pair of opposite chirality fields (1, 2), see Fig. 4(a1).

Also, $\mathcal{X}d$ is positive (1.9×10^{-2}) for the pair of electric fields (1,3) and negative (-1.8×10^{-2}) for the pair (2,3). Indeed, a close inspection of Fig. 4(a2) and Fig. 4(a3) shows that the probability distribution for Case 1 — Case 3 has mainly two spots in the third (yellow) and fourth (blue) quadrants while it is reflected with respect to the $p_y p_z$ axis for Case 2 — Case 3. We note that $1.9 \times 10^{-2} - 1.8 \times 10^{-2}$ is roughly zero, since pulses 1 and 2 have opposite chirality. Similar results are obtained when considering the chiral fields 4,5 and achiral field 6, see Figs. 4(b1)–4(b3).

IV. CONCLUSIONS

In conclusion, we identify a measure of chirality in electron ionization triggered in atoms driven by synthetic pulses. These pulses can create electric fields which are globally chiral or achiral along the focus region. We define this measure by multiplying the sign of the electron final momentum scalar triple product $\mathbf{p}_x \cdot (\mathbf{p}_y \times \mathbf{p}_z)$ with the probability for an electron to ionize with certain values of the electron momentum components. Finally, we integrate over all values of the electron momentum components appropriate reference frame. Choosing such frames has been a common practice in previous studies of circular dichroism and magnetic field effects.

ACKNOWLEDGMENTS

A.E. and G.P. Katsoulis acknowledge the use of the UCL Myriad High Throughput Computing Facility (Myriad@UCL), and associated support services, in the completion of this work. A.E. and G.P.K. acknowledge the EPSRC Grant No. EP/W005352/1. P.B.C. acknowledges funds from the U.S. Air Force Office of Scientific Research (AFOSR, FA9550-16-1-0109). A.S. acknowledges support from an NSERC Discovery Grant No. (RGPIN/05858-2020).

- [9] O. Neufeld, D. Ayuso, P. Decleva, M. Y. Ivanov, O. Smirnova, and O. Cohen, Ultrasensitive Chiral Spectroscopy by Dynamical Symmetry Breaking in High Harmonic Generation, Phys. Rev. X 9, 031002 (2019).
- [10] T. Heinrich, M. Taucer, O. Kfir, P. B. Corkum, A. Staudte, C. Ropers, and M. Sivis, Chiral high-harmonic generation

^[1] R. Cireasa, A. E. Boguslavskiy, B. Pons, M. C. H. Wong, D. Descamps, S. Petit, H. Ruf, N. Thiré, A. Ferré, J. Suarez, J. Higuet, B. E. Schmidt, A. F. Alharbi, F. Légaré, V. Blanchet, B. Fabre, S. Patchkovskii, O. Smirnova, Y. Mairesse, and V. R. Bhardwaj, Probing molecular chirality on a sub-femtosecond timescale, Nat. Phys. 11, 654 (2015).

^[2] S. Beaulieu, A. Comby, A. Clergerie, J. Caillat, D. Descamps, N. Dudovich, B. Fabre, R. Géneaux, F. Légaré, S. Petit, B. Pons, G. Porat, T. Ruchon, R. Taïeb, V. Blanchet, and Y. Mairesse, Attosecond-resolved photoionization of chiral molecules, Science 358, 1288 (2017).

^[3] S. Beaulieu, A. Comby, D. Descamps, B. Fabre, G. A. Garcia, R. Géneaux, A. G. Harvey, F. Légaré, Z. Mašín, L. Nahon, A. F. Ordonez, S. Petit, B. Pons, Y. Mairesse, O. Smirnova, and V. Blanchet, Photoexcitation circular dichroism in chiral molecules, Nat. Phys. 14, 484 (2018).

^[4] A. Comby, E. Bloch, C. M. M. Bond, D. Descamps, J. Miles, S. Petit, S. Rozen, J. B. Greenwood, V. Blanchet, and Y. Mairesse, Real-time determination of enantiomeric and isomeric content using photoelectron elliptical dichroism, Nat. Commun. 9, 5212 (2018).

^[5] S. Rozen, A. Comby, E. Bloch, S. Beauvarlet, D. Descamps, B. Fabre, S. Petit, V. Blanchet, B. Pons, N. Dudovich, and Y. Mairesse, Controlling Subcycle Optical Chirality in the Photoionization of Chiral Molecules, Phys. Rev. X 9, 031004 (2019).

^[6] D. Ayuso, O. Neufeld, A. F. Ordonez, P. Decleva, G. Lerner, O. Cohen, M. Ivanov, and O. Smirnova, Synthetic chiral light for efficient control of chiral light–matter interaction, Nat. Photonics 13, 866 (2019).

^[7] D. Baykusheva and H. J. Wörner, Chiral Discrimination through Bielliptical High-Harmonic Spectroscopy, Phys. Rev. X 8, 031060 (2018).

^[8] O. Neufeld and O. Cohen, Optical Chirality in Nonlinear Optics: Application to High Harmonic Generation, Phys. Rev. Lett. 120, 133206 (2018).

- and spectroscopy on solid surfaces using polarization-tailored strong fields, Nat. Commun. 12, 3723 (2021).
- [11] C. Lux, M. Wollenhaupt, T. Bolze, Q. Liang, J. Köhler, C. Sarpe, and T. Baumert, Circular dichroism in the photoelectron angular distributions of camphor and fenchone from multiphoton ionization with femtosecond laser pulses, Angew. Chem. Int. Ed. 51, 5001 (2012).
- [12] C. S. Lehmann, N. B. Ram, I. Powis, and M. H. M. Janssen, Imaging photoelectron circular dichroism of chiral molecules by femtosecond multiphoton coincidence detection, J. Chem. Phys. 139, 234307 (2013).
- [13] R. Boge, S. Heuser, M. Sabbar, M. Lucchini, L. Gallmann, C. Cirelli, and U. Keller, Revealing the time-dependent polarization of ultrashort pulses with sub-cycle resolution, Opt. Express 22, 26967 (2014).
- [14] A. Emmanouilidou and T. Meltzer, Recollision as a probe of magnetic-field effects in nonsequential double ionization, Phys. Rev. A 95, 033405 (2017).
- [15] L. D. Landau and E. M. Lifshitz, *Quantum Mechanics Nonrel-ativistic Theory*, 2nd ed. (Pergamon, Oxford, 1965).
- [16] N. B. Delone and V. P. Krainov, Energy and angular electron spectra for the tunnel ionization of atoms by strong low-frequency radiation, J. Opt. Soc. Am. B 8, 1207 (1991).
- [17] B. HuP, J. Liu, and S. G. Chen, Plateau in above-thresholdionization spectra and chaotic behavior in rescattering processes, Phys. Lett. A 236, 533 (1997).
- [18] R. Abrines and I. C. Percival, Classical theory of charge transfer and ionization of hydrogen atoms by protons, Proc. Phys. Soc. 88, 861 (1966).

- [19] P. Kustaanheimo and E. Stiefel, Perturbation theory of kepler motion based on spinor regularization, J. Reine Angew. Math. 1965, 204 (1965).
- [20] A. Emmanouilidou, Recoil collisions as a portal to field-assisted ionization at near-uv frequencies in the strong-field double ionization of helium, Phys. Rev. A 78, 023411 (2008).
- [21] J. S. Parker, B. J. S. Doherty, K. T. Taylor, K. D. Schultz, C. I. Blaga, and L. F. DiMauro, High-Energy Cutoff in the Spectrum of Strong-Field Nonsequential Double Ionization, Phys. Rev. Lett. 96, 133001 (2006).
- [22] A. Staudte, C. Ruiz, M. Schöffler, S. Schössler, D. Zeidler, Th. Weber, M. Meckel, D. M. Villeneuve, P. B. Corkum, A. Becker, and R. Dörner, Binary and Recoil Collisions in Strong Field Double Ionization of Helium, Phys. Rev. Lett. 99, 263002 (2007).
- [23] A. Rudenko, V. L. B. de Jesus, Th. Ergler, K. Zrost, B. Feuerstein, C. D. Schröter, R. Moshammer, and J. Ullrich, Correlated Two-Electron Momentum Spectra for Strong-Field Nonsequential Double Ionization of He at 800 nm, Phys. Rev. Lett. 99, 263003 (2007).
- [24] A. Emmanouilidou, J. S. Parker, L. R. Moore, and K. T. Taylor, Direct versus delayed pathways in strong-field non-sequential double ionization, New J. Phys. 13, 043001 (2011).
- [25] G. P. Katsoulis, A. Hadjipittas, B. Bergues, M. F. Kling, and A. Emmanouilidou, Slingshot Nonsequential Double Ionization as a Gate to Anticorrelated Two-Electron Escape, Phys. Rev. Lett. 121, 263203 (2018).
- [26] A. Chen, M. Kübel, B. Bergues, M. F. Kling, and A. Emmanouilidou, Non-sequential double ionization with near-single cycle laser pulses, Sci. Rep. 7, 7488 (2017).